Microfluidic study of effects of flow velocity and nutrient concentration on biofilm accumulation and adhesive strength in the flowing and no-flowing microchannels

Na Liu,[1] Tormod Skauge,[1] David Landa-Marbán,[2] Beate Hovland,[1] Bente Thorbjørnsen,[1] Florin Adrian Radu,[2] Bartek Florczyk Vik,[1] Thomas Baumann,[3] Gunhild Bødtker[1]#

[1]Uni Research, Centre for Integrated Petroleum Research (CIPR), Nygårdsgaten 112, 5008 Norway

[2]Department of Mathematics, Faculty of Mathematics and Natural Sciences, University of Bergen, Allégaten 41, P.O. Box 7803, 5020 Bergen, Norway.

[3]Institute of Hydrochemistry, Technische Universität München, Marchioninistr. 17, D-81377 München, Germany

#Address correspondence to Gunhild Bødtker, gubo@norceresearch.no

Abstract

Biofilm accumulation in porous media can cause pore plugging and change many of the physical properties of porous media. Engineering bioplugging may have significant applications for many industrial processes, while improved knowledge on biofilm accumulation in porous media at porescale in general have broad relevance for a range of industries as well as environmental and water research. The experimental results by means of microscopic imaging over a T-shape microchannel clearly show that increase in fluid velocity could facilitate biofilm growth, but that above a velocity threshold, biofilm detachment and inhibition of biofilm formation due to high shear stress were observed. High nutrient concentration prompts the biofilm growth, however the generated biofilm displays a weak adhesive strength. This paper provides an overview of biofilm development in a hydrodynamic environment for better prediction and modelling of bioplugging processes associated with porous systems in petroleum industry, hydrogeology, and water purification.

Keywords

Microfluidics · Flow velocity · Nutrient concentration · Biofilm accumulation · Adhesive strength

Introduction

Biofilm accumulation in the pore space can cause pore plugging (bioplugging), leading to significant changes in physical properties of porous media by reduction of porosity and permeability [8,34,47]. The plugging effect might have negative impacts in many industrial and medical applications because the plugging of pores require extra cost to clean, mitigate and prevent. However, engineering bioplugging have been explored as a viable technique for various practices, such as in situ bioremediation [19], soil injection [32], waste treatment [6], water treatment [12] and microbial enhanced oil recovery (MEOR) [16,21,22,35]. In MEOR technology trails, selective biofilm accumulation in high permeability zones of the reservoir leads to the diversion of injection fluids towards lower permeable oil filled zones to improve the oil recovery [3,13,38]. Bioplugging strategy has been proven to be efficient for improving water flood efficiency and oil recovery based on various studies. Fujiwara et al. [13] showed that the bacterial strain CJF-002 was able to attach and form biofilm on the reservoir rock, and when injected into the oil reservoir followed by injection of growth substrate (molasses), it selectively grew and formed bio plugs in the high permeable zones of the reservoir. Enhanced recovery was observed by an increase of oil production and concomitant reduction in water cut. Suthar et al. [44] confirmed the obtained oil recovery in the sand pack column because of the anaerobic bacterial *Bacillus licheniformis* TT33 growth and biomasses formation in highly permeable zones. Klueglein et al. [24] studied the effects of nutrient concentrations on growth and agglomeration of MEOR microorganisms present in the original injection water from a Wintershall oil field.

MEOR bioplugging technologies aim to control specific microorganisms attaching and forming biofilm at desired parts of a reservoir, in order to achieve improved sweep to improve oil production. However, unspecific microbial growth in the near wellbore area may have potential negative consequences such as formation damage and reduced injectivity [10,50]. Microbial growth in reservoir formations is dependent on nutrient availability, and studies have shown that many chemical injection water additives applied by the oil industry, may be utilized by native microorganisms as growth substrate [43]. Furthermore, on-site coreflood experiments at Prudhoe Bay field (Alaska) suggests that reinjection of pre-filtered produced water may cause injectivity damage due to bacterial growth [17]. Therefore, application of engineering bioplugging requires knowledge on how to control bacterial growth. Even though tremendous efforts have

been made to prove the efficiency of bioplugging strategies, the deep mechanisms of biofilm formation and development in porous media at porescale, are rarely reported. Likewise, biofilm-induced formation damage have been studied and reported [50], but the need to also study the basic mechanisms involved at pore scale is necessary in order to understand and simulate bioplugging at Darcy and field scale. Hydrodynamic conditions are the most important parameters affecting the formation of bioplugging in porous media as biofilm growth and detachment could be significantly influenced by the surrounding environment, including shear stress, nutrient status, temperature, pH, and so on [15,28,41]. Biofilm growth and detachment rates could both increase with injection velocity, as the increased mass transfer facilitates nutrients supply for bacterial growth, while the increased shear force in turn cause detachment [7,28,48]. There is a consensus that biofilm growth rate increases with nutrients concentration, while nutrient starvation results in biofilm detachment [4,18,36]. Therefore, the primary objective of this paper is to describe a correlation between biofilm accumulations and its adhesive strength and hydrodynamic conditions like flow velocity and nutrient concentration, to improve the understanding of bioplugging in general.

Traditionally quiescent experiments for biofilm formation and transport research are normally carried on homogeneous physical conditions, which lack environmental complexities for accurately determining the dynamic changes occurring during biofilm development [37]. The advent of new technologies, specially microfluidics, have attracted a rapidly growing interest to emulate biological phenomena by addressing unprecedented control over the flow conditions, providing identical and reproducible culture conditions, as well as real-time observation [4,39,45]. Indeed, there are few reports related to use microfluidics for observing biofilm formation and transport at porescale under various hydrodynamic conditions [25,49]. Dunsmore et al. [9] injected the sulphate-reducing bacterium, *Desulfovibrio sp.* EX265, into a glass micromodel and observed a decrease in permeability due to biofilm accumulation in the pore and blocking pore throats. Karambeigi et al. [20] used a glass micromodel with two different heterogeneities to investigate the potential of bioplugging to improve the efficiency of water flooding. An improved oil recovery in high permeable zones was observed by injection of a mixed culture of oil degrading microorganisms into porous media. Park et al. [33] presented effects of shear stress on biofilm formation in a microfluidic channel, and confirmed that under the optimum shear stress, biofilm could resist the flow-

induced shear stress by forming a stable extracellular polymeric substance (EPS) structure to provide a mechanical shield. Zhang et al. [51] designed a microfluidic gradient mixer to monitor biofilm development as response to a defined calcium and nitrate gradients. These studies demonstrate that the microfluidic device coupled with a microscope is an effective tool for in situ analysis and quantification of biofilm formation and transport in porous media at porescale. Herein, we used a T-shape microfluidic device equipped with a microscope to study the biofilm accumulation and adhesive strength as responds to various flow velocities and nutrient concentrations in the microchannel.

Materials and methods

Bacteria and fluids

The bacterium used in the study was: *Thalassospira* strain A216101, a facultative anaerobic, nitrate-reducing bacteria (NRB), capable of growing under both aerobic and anaerobic conditions. It is able to grow on fatty acids and other organics acids as sole carbon and energy source. The bacterium was cultured in a marine mineral medium, which contained the following components (l^{-1}): 0.02 g Na_2SO_4, 1.00 g KH_2PO_4, 0.10 g NH_4Cl, 20.00 g NaCl, 3.00 g $MgCl_2 \cdot 6H_2O$, 0.50 g KCl, 0.15 g $CaCl_2 \cdot 2H_2O$, 0.70 g $NaNO_3$, and 0.50 ml 0.20% resazurin [30]. Resazurin dye is a redox indicator that was added to the growth medium in order to evaluate the metabolic activity in the microchannel by simple visual inspection of the effluent produced. Respiratory growth irreversibly reduce the blue colored resazurin to pink colored resorufin. The medium is hereafter referred to as growth medium. After autoclaving in a dispenser, 1 liter of growth medium was added 5 ml vitamin solution and 20 ml 1 M $NaHCO_3$ to adjust the pH to 7.00 ± 0.10. Finally, pyruvate was added as the carbon source from a sterile stock solution to achieve final nutrient concentrations of 20 mM, 10 mM, 5 mM, and 1 mM, respectively. The final nutrient medium was stored at 4°C.

Experimental setup

The experimental apparatus is illustrated in Fig. 1 (a). A glass T-junction microfluidic device (Micronit, Netherland) consists of a single straight channel and a side channel with the sizes of 100 μm width and 20

μm depth and the nuzzle size at the cross-section as narrow as 10 μm (Fig. 1 (b)). Two syringe pumps (NE-1000 Series of Syringe Pumps, accuracy ±1%) were used to load the bacterial solution and nutrients solution separately into microchannels. The light source is a cold halogen lamp with 24v, 150w, placed under the microchip for better illumination. A microscope with a digital camera (VisiCam 5.0, VWR) was used to acquire image sequences. Measurements and experiments were conducted at ambient temperature and pressure.

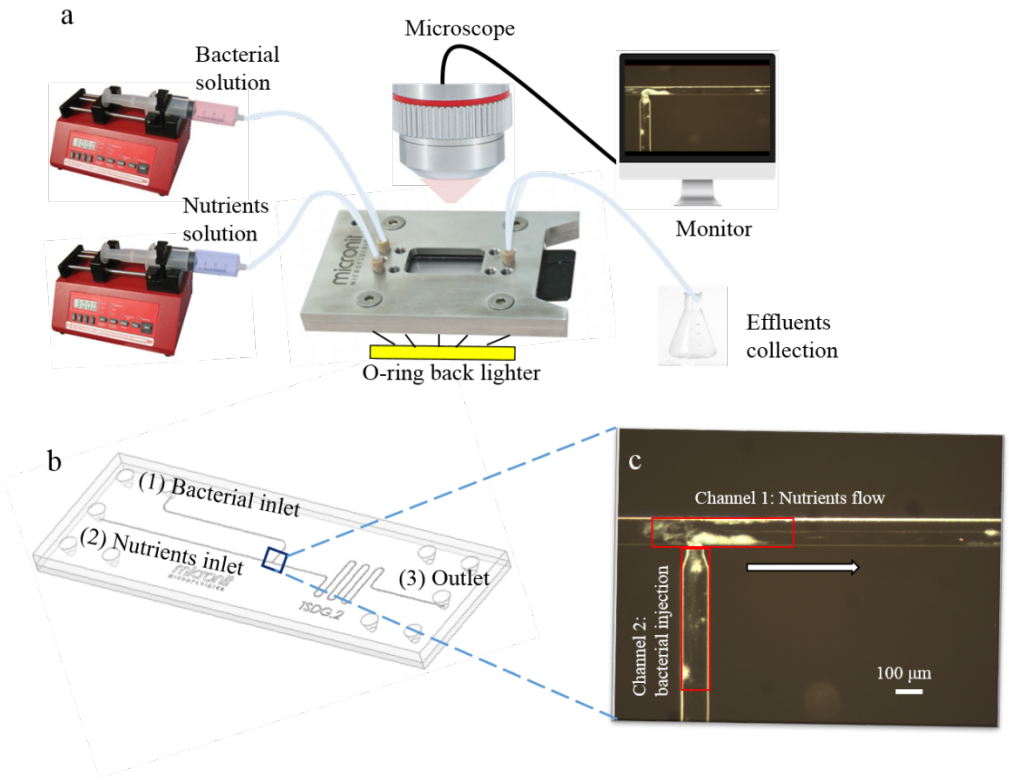

Fig. 1 (a) Schematic illustration of the experimental setup; (b) The glass T-shape microchannel in this study contains two inlet ports (1 Bacterial inlet and 2 Nutrients inlet) and one outlet port (3). Microchip image comes from Micronit website; (c) Image of biofilm growth recorded by microscope. Flow direction from left to right.

Inoculation process

Before inoculation, the microchannel was cleaned using ethyl alcohol, deionized water, H_2O_2 solution (10% w/w) and deionized water to guarantee the same surface condition for each experiment. The bacterial inocula were pre-cultured in the growth medium containing 10 mM nutrients at 30 °C for 24 h. The initial

cells density of the inoculum was approximately 1 x 10^9 cells/ml. Inoculation was achieved by injecting the pre-culture bacterial solution from the bacterial inlet port (Fig. 1 (b)) into the side channel (Channel 2) at the rate of 1.0 µl/min for 24 h, followed by a 24 h shut-in period. In case of biofilm plugging the nutrients flow channel (Channel 1), we closed the nutrient inlet during inoculation to force the bacterial solution to only flow towards the outlet direction. Then only growth medium, with various pyruvate concentrations from 1 mM to 20 mM, were injected into Channel 1 from the nutrients inlet at constant flowrates from 0.2 to 0.5 µl/min, while Channel 2 was closed, which led to a greater growing of bacteria on the surface of the intersection of straight channel and side channel (Fig. 1 (c)). After nutrient flooding, the microchannel was rinsed with ethyl alcohol, water, H_2O_2 solution and water separately, finally, filled with the marine medium without nutrients until the onset of the next experiment.

Image process

Image sequences on biofilm growth were acquired with a Leica microscope fitted with a digital camera for scoring with time. The main area of interest in this study is the intersection of straight channel and side channel, thereby two areas of interest (AOIs) with 0.5mm*0.1mm are extracted from the origin image for further image analysis (Red squares in Fig. 1 (c)). The image processing was performed using MATLAB®'s Image Processing Toolbox. Biofilm accumulation, here presented by biofilm coverage (A_{nt}) in areas of interest, was periodically measured in a flowing channel (Channel 1) and no-flowing channel (Channel 2). Further details on image process can be found in Support Information.

Quantitative real-time PCR (qPCR)

Fluid samples were collected daily at the outlet for analysis by quantitative real-time PCR (qPCR) in order to determine the total cell number produced and/or released from the biofilm. Amplification of the V3 region of 16S rRNA gene was performed by use of *Bacteria* primer PRBA338f (5′-ACTCCTACGGGAGGCAGCAG-3′) [27] and Universal primer PRUN518r (5′-ATTACCGCGGCTGCTGG-3′) [29]. The template for the reaction was DNA from whole cells, pre-treated by freezing and thawing in order to open the cells and allow DNA amplification. A 20 µl qPCR reaction mix containing 10 µl QuantiTect® SYBR® Green PCR kit (Qiagen, Germany) 0.06 µl primers (100µM),

8.88 µl nuclease free water (Qiagen, Germany) and 1 µl cell template was prepared in 0.2 ml low-profile 8-strip white PCR tubes covered with optical flat 8-cap strips (Bio-Rad Laboratories, USA) . The reaction was run at the following cycling conditions: initial activation at 95°C for 15 minutes, 36 cycles with denaturation for 30 seconds at 94°C, annealing for 30 seconds at 55°C, extension for 1 minute at 72°C followed by a plate read. At the end, a melting curve from 55°C to 95°C was conducted. The reactions were carried out in a CFX connect™ real time PCR detection system (Bio-Rad Laboratories, USA). Each run included two parallel analysis of each sample and standards (prepared from isolated DNA of *Thalassospira* cells, 5 times 10 fold diluted). The number of amplicons were divide by the factor 3.8 to correct for the average number of 16S rRNA copies in bacteria [42]. The qPCR results are given as the mean ± standard deviation (SD) of the two individual analyses.

Results

Effects of flow velocity on biofilm accumulation and adhesive strength

After inoculation, four sets of nutrient flooding experiments with 10 mM pyruvate concentration were conducted at various injection rates (0.2, 0.3, 0.4 and 0.5 µl/min) to measure effects of injection velocity on biofilm accumulation in microchannels. After 6 days of nutrient flooding, the flowrate was increased stepwise by 0.1 µl/min for 1 h, until up to 1.2 µl/min, to test the adhesive strength of biofilm attached on the solid surface. The corresponding flow velocity, Peclet number, Reynolds number and Shear rate at each flowrate in Channel 1 are listed in Table 1. The Peclet number is the ratio of heat transfer by convection to heat transfer by conduction within the fluid. The Reynolds number is the ratio of the inertial forces to the viscous forces. Shear rate is the velocity gradient across the diameter of the fluid-flow channel. The accumulation of biofilm at different velocities was observed and registered as function of time by use of microscope.

Table 1 Table of basic flow parameters at various flowrates in this study.

Flowrate, µl/min	**Velocity, mm/s**	**Peclet number, Pe**	**Reynolds number, Re**	**Shear rate, s^{-1}**

0.2	1.66	97.64	0.17	83.33
0.3	2.50	147.06	0.25	125.00
0.4	3.33	195.88	0.33	166.67
0.5	4.17	245.30	0.42	208.33
1.2	10.00	705.88	1.00	500.00

Biofilm morphologies

Images of biofilm development in nutrients flowing channel (Channel 1) and no-flowing channel (Channel 2) at various flow velocities are shown in Fig. 2. It is noticed that biofilm in Channel 1 reveals different morphological characters involving coverage and shape depending on flow velocities. After inoculation, the initial attached biomasses at low velocities (1.66 and 2.50 mm/s) became irreversible and developed towards different structures of biofilm along the growth medium flow. Biofilm at 1.66 mm/s tends to be approximately circular shape and has a larger coverage area, while biofilm at 2.50 mm/s shows an appearance of thin plate structure. There is no clear biofilm formation in Channel 1 at high velocities (3.33 and 4.17 mm/s), which indicates that shear forces imposed at high flow velocities were larger than the adhesion forces between biofilms and surfaces.

On the contrary, biofilm formed in Channel 2 at 3.33 mm/s led to the largest cluster compared with low velocities, indicating that hydrodynamic conditions in Channel 1 determined the flux of nutrients transport to Channel 2, and high shear stress in Channel 1 facilities mass transfer in Channel 2 and stimulates bacterial growth. Noteworthy is that in the case of injection velocity of 1.66 mm/s, biofilm continued developing to some extent in Channel 2 when the nozzle was plugged by biofilm accumulation in Channel 1, which is likely because the formed biofilm was permeable to nutrients. There was no biofilm growth in either channel at the highest flow velocity of 4.17 mm/s, which suggests that the high shear forces may prevent biofilm formation. This result is in agreement with industrial applications where the formation of biofilm is prevented by high velocity flooding [14].

After 6 days of injection at a constant rate, the injection rate was increased stepwise by 0.1 μl/min, until up to 1.2 μl/min (corresponding 500.00 s^{-1} of shear rate), to test the adhesive strength between biofilm and the

191 solid surface. As shown in the right column images of Fig. 2, biofilm in Channel 1 at 1.66 mm/s became
192 elongated in the flowing direction to form filamentous "streamers" when increasing the shear rate.
193 However there were no clear biofilm shape differences in cases of higher flow velocities (2.50 and 3.33
194 mm/s).

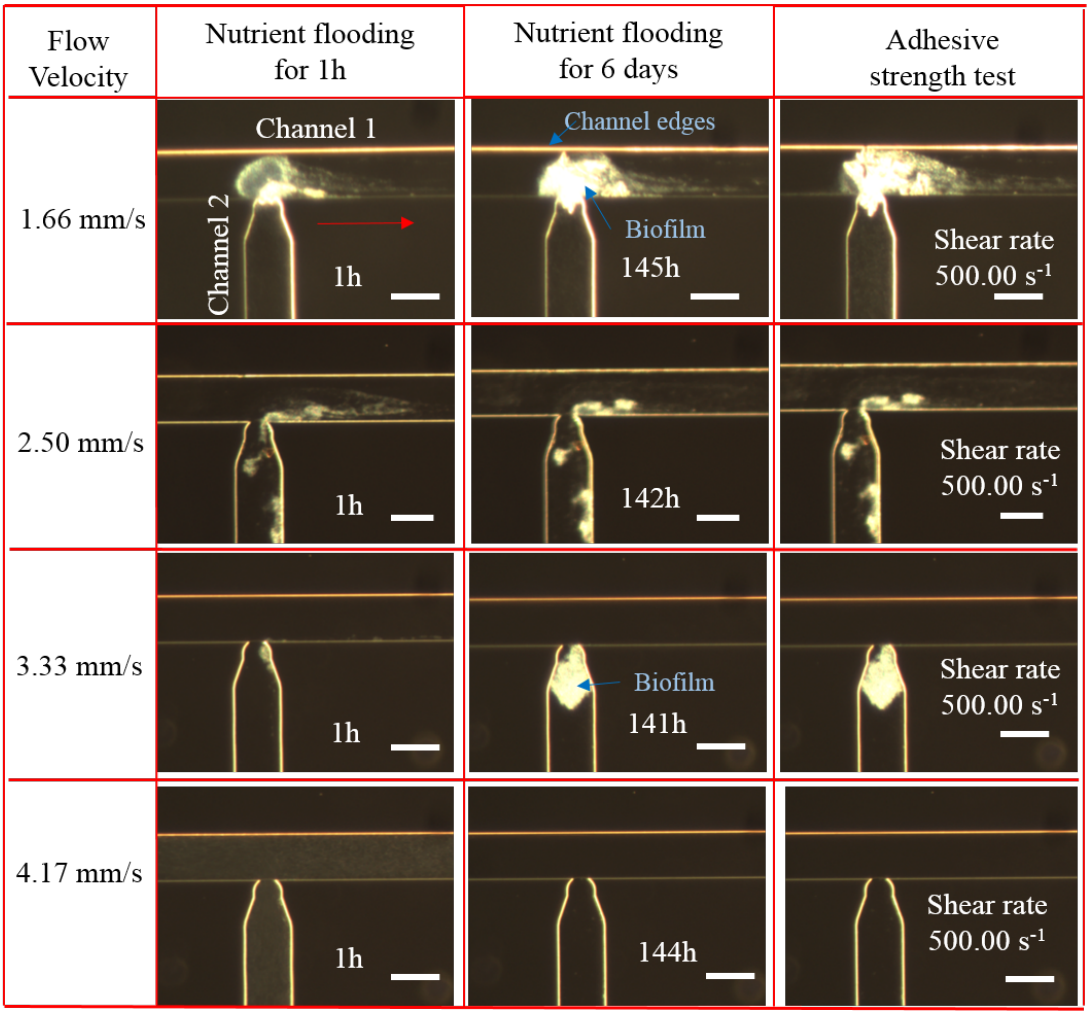

195

196 **Fig. 2** Optical images of biofilm growth in both microchannels at 10 mM and various velocities. As shown
197 in images, biofilm features, and channel edges are bright and the surrounding voids dark. The first column
198 of images compared biofilm development in microchannels at different flow velocities for 1 h. After
199 continually injecting growth medium at constant flowrates for around 6 days, images of biofilm in
200 microchannels are shown in the middle column. The right column shows the response of biofilm at high
201 flowrate of 1.2 µl/min, corresponding the shear rate of 500.00 s^{-1}. Nutrients flow from left to right in the
202 upper channel. Scale bars indicate 100 µm.

Biofilm accumulation in the flowing and no-flowing channels

Biofilm coverages as a function of time for different flow velocities in two microchannels are listed in Fig. 3. In Channel 1 (Fig. 3 (a)), the coverage of biofilm decreased in the first 24 h as the flow shear stress snapped off some of weak initial attachments. When the left biofilm turned into irreversibly attached and new biofilm formed, biofilm coverage increased over time. Fig. 3 (a) shows more biofilm accumulation in Channel 1 at low flow velocities. Fig. 3 (b) plots biofilm coverage in the no-flowing channel (Channel 2) as a function of time in each run. Biofilm coverages at all velocities increased over time, while the optimum velocity is 3.33 mm/s due to its exceptionally high accumulation rate. This might attribute to that biofilm growth in the no-flowing Channel 2 was highly dependent on the nutrient diffusive flux from the nurtrient-flowing Channel 1, where the high velocity in Channel 1 facilitated the nutrients transportation from Channel 1 to Channel 2. In the case of the highest flow velocity of 4.17 mm/s, there was few cells attached in areas of interest (AOIs) after nutrient flooding (Fig. 2), which might cause less active cells for further biofilm growth in AOIs. Therefore, the velocity of 3.33 mm/s leaded to the largest biofilm accumulation compared to other flow velocities.

Comparing biofilm growth at 2.50 mm/s in the nutrient flowing channel and no-flowing channel in Fig. 3 (c), biofilm coverage in two channels increased with time initially. However, after 75 hours biofilm coverage in Channel 2 reached to a plateau value, while biofilm coverage in Channel 1 continued increasing over time. The stable coverage obtained in Channel 2 might be attributed to that cells within the biofilm cannot obtain sufficient essential sources of nutrients for producing new biofilm as bacterial cells dramatically increased in the growing biofilm community. However, the continuous nutrients supply in Channel 1 leads to a delay of this leave-off behavior. Fig. 3 (d) compares the experimental data (dots) with the mathematical model (lines) of biofilm coverages in both microchannels at various velocities. The numerical data is from D. L. Marbán' work [26] and shows that our experiment data is well fit with the numerical simulation. The mathematical model considered the biofilm as a porous medium and formed by water, EPS, active, and dead bacteria. The flow of free water was modelled by the Stokes equation, whereas the flow of water inside the biofilm was modelled by the Brinkman equation. A diffusion-convection equation was involved for the transport of nutrients. The location of the biofilm-water interface changed in

time due to detachment of biomass, as well as due to reproduction of bacteria, production of EPS, and bacterial decay.

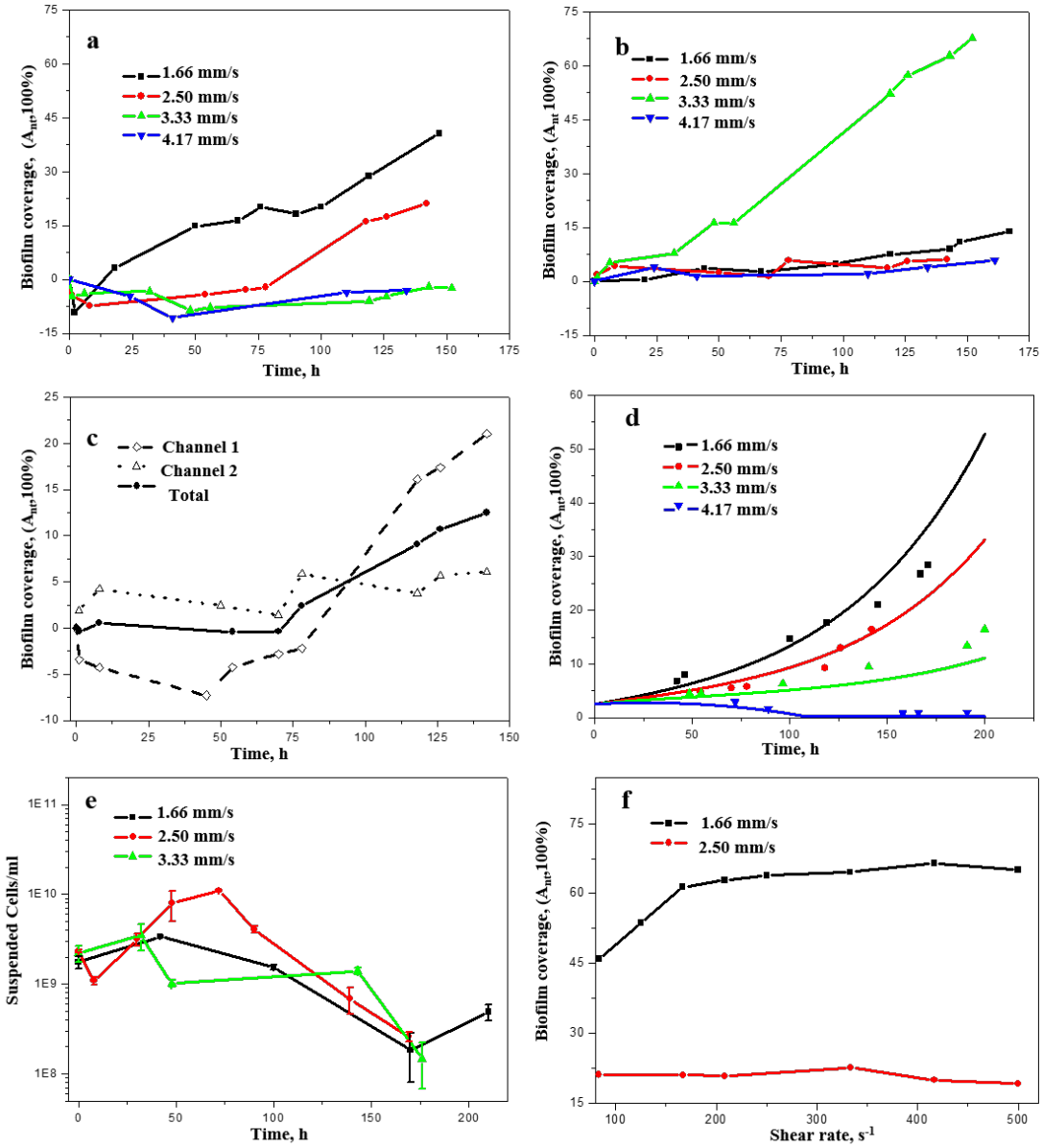

Fig. 3 (a) Biofilm coverage over time in Channel 1 at various velocities; (b) Biofilm coverage over time in Channel 2 at different velocities; (c) Comparison of biofilm accumulation in both channels at 2.50 mm/s; (d) Experimental data and numerical simulations of biofilm coverage in both channels at various velocities; (e) Number of released cells as a function of biofilm culture time at various velocities (Error bars are ±

standard deviation); (f) Biofilm coverage in Channel 1 as response to the increasing shear rate after bacterial growing at the velocities of 1.66 and 2.50 mm/s for 6 days.

Biofilm adhesive strength test

Fig. 3 (e) shows the results of qPCR analysis of cell number in the effluent at various velocities. The cell number in effluent increased in the first 48h after inoculation, which mainly contributes to that the reversible adhered bacteria were driven out the microchannel by the shear stress. After nutrient flooding for 48h, cell number in effluent decreased over time, exhibiting that more bacteria involved into the biofilm construction. Since there were no bacterial injection during flooding, the measured cells in the effluent can be interpreted as the detachment of biofilm due to the flow-induced shear stress and/or planktonic cell growth in the bulk fluid.

For the adhesive strength test, biofilm coverages in Channel 1 as responds to the increasing shear rate from 83.33 s^{-1} and 125.00 s^{-1} up to 500.00 s^{-1} are shown in Fig. 3 (f). In the case of biofilm formation at 1.66 mm/s, its coverage area increased slightly when increasing shear rate up to 166.67 s^{-1}, suggesting that the increasing shear stress facilitates the diffusion of nutrients inside of biofilm and promotes its growth. However, according to the decrease of slope in the biofim coverage curve (Fig. 3 f), biofilm growth slowed down after continuely increasing the shear rate. When the shear rate was increased to 500 s^{-1}, biofilm coverage started to decrease, which might be explained by the detachment rate exceeding the growth rate. Simillar results were obtained for biofilm growth at flow velocity of 2.50 mm/s, where biofilm coverage increased at lower flow shear rates and decreased at higher shear rates.

Effects of nutrient concentration on biofilm accumulation and adhesive strength

Biofilm developments in channels were compared at four different nutrient concentrations to evaluate the effects of nutrient conditions on biofilm accumulation and adhesive strength. The baseline was 10 mM pyruvate in the growth medium and variations of two times (20 mM), half (5 mM) and one tenth (1 mM) of the baseline concentration were applied. Injections were performed at a constant velocity of 1.66 mm/s from Channel 1 for approximately 7 days, and followed by biofilm strength tests via steadily increasing shear rate. The images are shown in Fig. 4.

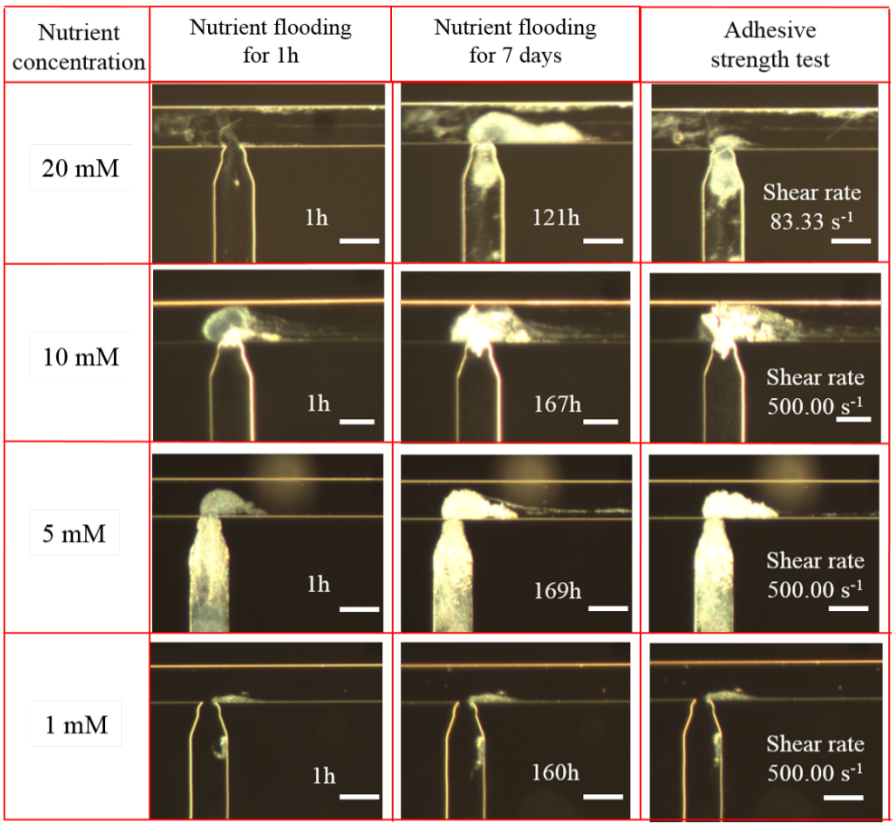

Fig. 4 Optical images of biofilm growth over time at various nutrient concentrations. The first column images compared biofilm development in microchannels at various nutrient concentrations for 1 h. The middle column shows images of biofilm growth after continually injecting nutrient solution for around 7 days. The right column lists the results of biofilm detachment on adhesive strength test by increasing shear rate up to 500.00 s^{-1}. Nutrient flow from left to right in the upper channel. Scale bars indicate 100 μm.

Biofilm morphologies

As shown in Fig. 4, biofilm in Channel 1 with the highest concentration 20 mM has a long, thick but loose structure, which is highly sensitive to the variation of shear stress. After 122 h, the formed biofilm detached from the channel surface, leaving behind a few attached biofilm spots to regrow. At nutrients input of 10 mM and 5 mM, biofilm became denser and compacted, and no detachment occurred with biofilm expansion. When reducing the nutrient concentration to 1 mM, there was no clear biofilm growth occurring in the nutrient flowing channel.

Biofilm in Channel 2 at nutrient inputs of 20 mM has larger coverages than other concentrations, which confirms that high nutrient concentrations supply could lead to a fast biofilm growth. The massive biofilm accumulation at low nutrient concentration of5 mM might be related to the large initial attachments containing more biomasses for biofilm development. It is noticed that there is barely new biofilm formation at both channels at 1 mM, which shows that the lowest nutrient input significantly limited new biofilm formation.

As responding to the increasing shear rate, the biofilm with low density and loose structure at 20 mM, was highly sensitive to the variation of shear stress, which detached from the substrate at the shear rate of 83.33 s^{-1}. Biofilm growth at 5 mM reacted as same as that at 10 mM to the increasing shear rate, which only the biofilm shape became elongated in the flowing direction but without large detachment.

Biofilm accumulation in the flowing and no-flowing channels

Biofilm coverages as a function of time for different nutrient concentrations in two microchannels are shown Fig. 5. As shown in Fig. 5 (a), biofilm growth in Channel 1 at a high nutrient concentration of 20 mM has a much faster accumulation rate in the first 5 days, but rapidly decreases to near zero when most parts of biofilm detached from the matrix. At the medium nutrient feeding zones (5 mM and 10 mM), biofilm coverage at 5 mM is higher than that of 10 mM in the first two days, but reached a plateau value after around 60 h. Thereby biofilm coverage reached a stable plateau when the low nutrient concentration limited further growth, At the lowest nutrient concentration of 1 mM, there was no clear biofilm formation in both channels. Therefore, the lowest nutrient concentration (1 mM) could not provide a proper environment for biofilm growth. In this study, the limiting nutrient concentration for biofilm growth appears to be between 1 mM and 5 mM.

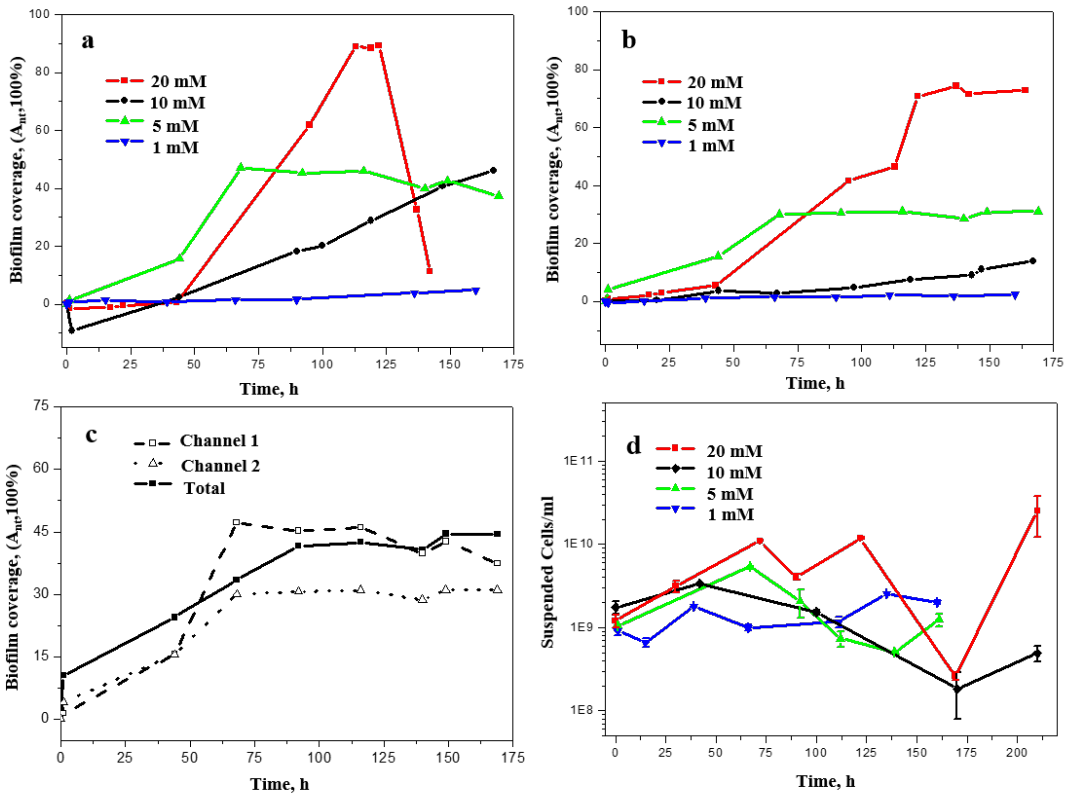

297

298 **Fig. 5** (a) Biofilm coverage over time in Channel 1 at different nutrient concentrations; (b) Biofilm
299 coverage over time in Channel 2 at different nutrient concentrations; (c) Comparison of biofilm coverage in
300 both channels at 5 mM and 1.66 mm/s; (d) Cell number of effluents at various nutrient concentrations at the
301 flow velocity of 1.66 mm/s (Error bars are ± standard deviation).

302 As shown in Fig. 5 (b), biofilm accumulation in Channel 2 is highly influenced by nutrient concentrations.
303 Biofilm formation at 20 mM has a faster accumulation rate than other cases, indicating that the high
304 nutrient concentration in Channel 1 leads to an increase of biofilm growth in Channel 2. However, biofilms
305 at all the nutrient concentrations reach stable plateaus after 5 days when the growing biofilm community
306 could not obtain sufficient essential nutrients for further growth. The time to reach the stable plateau at 20
307 mM is later than 5 mM, suggesting that the high nutrient concentration leads to a decrease in the time taken
308 to reach the stable plateau in a no flow system. Fig. 5 (c) compares biofilm accumulation in both channels
309 at 5 mM. Apparently, the time to reach the plateau in Channel 1 was later than that in Channel 2, indicating
310 that the flow shear rate in Channel can facilitate mass transfer and lead an increase in the time taken to

311 reach the stable state. These results confirm that nutrient availability has a significate influence on biofilm
312 development.

313 *Biofilm adhesive strength test.*

314 Fig. 5 (d) presents the results of the cell number in the effluent at four different nutrient concentrations.
315 Apparently, the released cell number at 20 mM is higher than those at lower nutrient concentrations, which
316 might be contributed to that the high nutrient supply promote a higher planktonic growth. The number of
317 released/detached cells is relatively in the same level at 5 mM and 10 mM in the first 5 days. However,
318 when biofilm stopped growing at 5 mM (the plateau in Fig. 5 (c)), the detached cells increased over time,
319 suggesting that the mature biofilm would disperse more planktonic cells into the bulk liquid [28]. At the
320 limited nutrient supply (1 mM), the released cell number in the effluent was stable during nutrient flooding.
321 In the case of no biofilm formation in channels (Fig. 4), bacteria at limited nutrient supply might prefer to
322 live in the planktonic style instead of biofilm style [1].

323 It is noticed that biofilm growth at 20 mM has a weak adhesive strength with the substrate, because cells
324 deep in the biofilm were dispersed from the interior of the biofilm matrix causing large degree of
325 detachment. We also observed this dispersion occurring at flow velocity of 2.50 mm/s (Fig. 6). A central
326 region of the biofilm matrix (the red circles in Fig. 6 (a)), became visible and light after a few days of
327 biofilm growth, which has demonstrated as the pre-dispersion behavior [11]. Then microcolonies within the
328 regions migrated into the bulk liquid, leading to huge biofilm detachments. Biofilm were observed to
329 undergo growth and dispersion simultaneously at the highest nutrient concentration (Fig. 6 (b)). As biofilm
330 growth at a fast accumulation rate at 20 mM, cells trapped in the deep of biofilm matrix have difficulties to
331 obtain essential sources of energy or nutrients via diffusion from the bulk solution to the biofilm structure.
332 In addition, waste products and toxins accumulated also in a high speed inside the biofilm community.
333 When they reached toxic levels to threaten cells survival, microorganisms would be released from the deep
334 of the biofilm matrix to resettle at a new location to develop again.

a

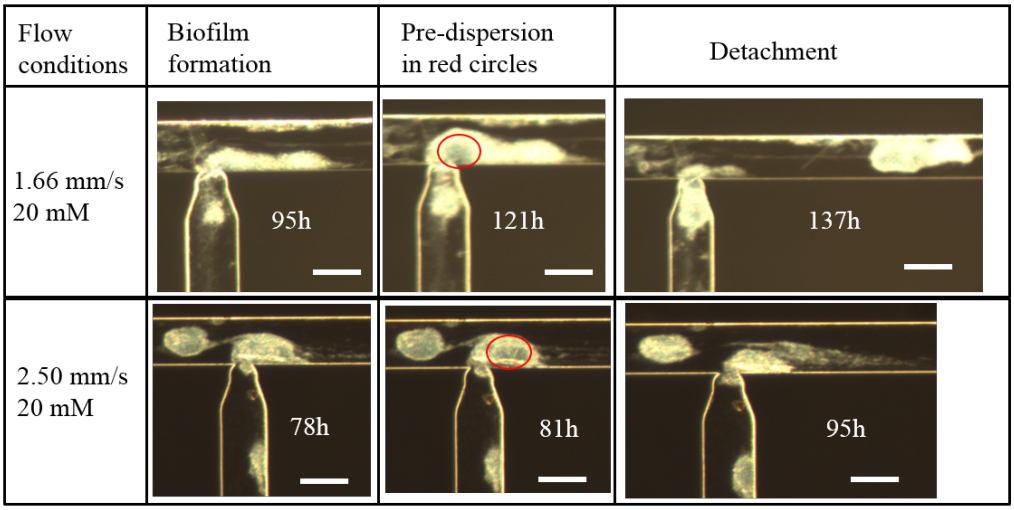

b

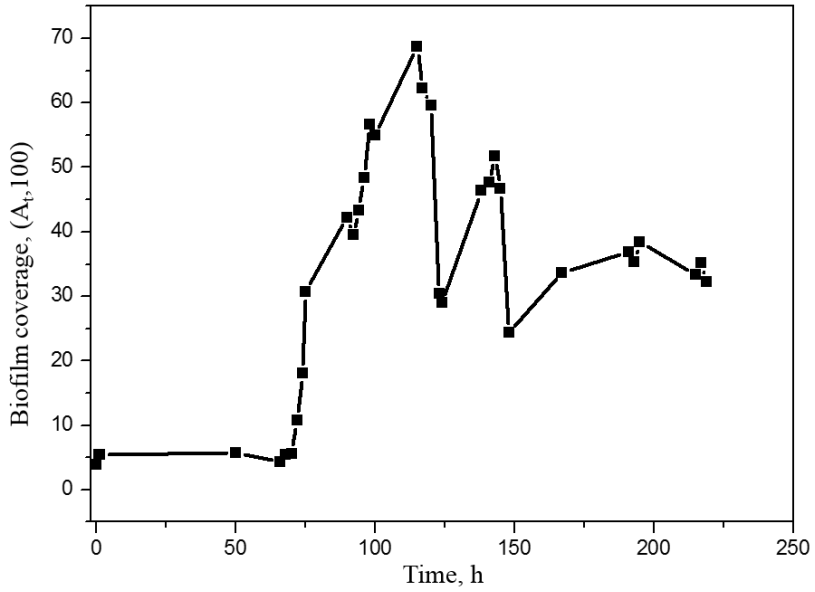

335

336 **Fig. 6** (a) Images of biofilm growth following dispersion events at high nutrient concentration of 20 mM
337 and flow velocities at 1.66 and 2.50 mm/s. Red circles at two images of 121h and 81h demonstrate the pre-
338 dispersion behavior. Flow direction from left to right. (b) Biofilm accumulation at 1.66 mm/s and nutrient
339 concentration of 20 mM.

Discussion

Biofilm morphologies

Observations on biofilm morphologies in both flow and no flow channels of each run demonstrate that flow velocity and nutrients concentration have direct effects on biofilm morphology. Shapes of biofilm in the nutrient flowing channel (Channel 1) shown the influence of flow drag in the direction of flow velocity, where the biofilm clusters became compacted and progressively elongated with the increase of flow velocity (Fig. 2). The biofilm at the high nutrient concentration had a long, thick but loose structure, while it turned to be denser and compacted at low nutrient concentrations (Fig. 4). Similar results have been reported in previous work [41].

Biofilm growth in Channel 2 is highly dependent on the diffusion of nutrients in Channel 1. As the former bacteria injection path, most parts of Channel 2 were full of biomasses without fluid shear forces. Only the void in the nozzle connecting with Channel 1 could act as the transport channel supplying nutrients for biofilm growth. Biofilm growth at the high shear rate of 166.67 s^{-1} and high nutrient concentration of 20 mM led to a larger cluster compared with others, indicating that high shear rate and nutrient concentration in Channel 1 facilitated the mass transfer of nutrients into Channel 2, and promoted biofilm growth in Channel 2. It is noticed that there was no biofilm growth in either channel at the highest flow velocity of 4.17 mm/s and lowest nutrients concentrations of 1 mM, suggesting that the high shear forces and limited nutrients loading may prohibit biofilm formation.

Biofilm accumulation

In this study, we set the initial biofilm coverage after inoculation to zero, and plotted the biofilm coverage (A_{nt}) by subtracting the initial attachment from all image sequences to analysis biofilm net accumulation rate during nutrient flooding. As shown in Fig. 3 (a) and Fig. 5 (a), the coverages of biofilm in Channel 1 are under zero in the early stage of injection, which demonstrates that the shear stress caused by nutrient flooding leads to the snap-off of weak initial attachments. When the remained biofilm became irreversibly attached, cells within biofilm behaved as nuclei for new bacteria/biofilm growth, resulting in the increase of biofilm coverage. Biofilm accumulation in the flowing microchannel (Channel 1) is highly related with

366 flow velocities through two important factors, mass transfer and shear stress [46,48]. As shown in Table 1,
367 the Reynolds numbers in Channel 1 were very low (from 0.17 to 0.42), while the mass transfer Peclet
368 number were extremely high (from 97.64 to 245.30), which suggests that mass transfer in the microchannel
369 was dominated by convective actions and has negligible diffusion during nutrient flooding [23]. Thereby,
370 the diffusion of nutrients from bulk to biofilm rarely increased with the increase of flow velocity, while the
371 shear stress by water flow increased linearly. The accumulation of biofilm, which is equal to its growth rate
372 minus detachment rate, decreased with the increase of flow velocities when the shear stress induced
373 detachment rate exceeding growth rate. Thereby, the optimum flow velocity for biofilm growth in the flow
374 microchannel is the lowest velocity of 1.66 mm/s in this work. Considering effects of nutrient
375 concentration, the biofilm accumulation in Channel 1 was linearly increased with nutrient concentrations.
376 Apparently, the highest nutrient concentration (20 mM) led to a much faster biofilm accumulation rate. The
377 similar biofilm growth rate at 5 mM and 10 mM implies that in a range of nutrient concentrations, the
378 biofilm growth rate is independent of nutrient status in the initial state of biofilm growth [36]. As biofilm
379 grows in size, the number of cells within the biofilm increases dramatically, resulting in their demands for
380 nutrients growing. Thereby the low nutrient concentration would limit growth in the later stage of biofilm
381 development.
382 Biofilm accumulation in Channel 2 increased with shear rate and nutrient concentration in Channel 1
383 monotonically. Due to an absence of shear stress, biofilm growth in Channel 2 depended on the nutrient
384 diffusive flux of Channel 1, where the flow shear rate and nutrient concentration could facilitate mass
385 transfer, leading to an increase in biofilm accumulation. Therefore, for a confined no flowing system,
386 biofilm accumulation rate is highly related to the nutrients availability, which are in correspondence with
387 previous works.
388 The results above indicate that for porous systems, like oil reservoirs, biofilm could develop not only in the
389 main water flow paths, but also in dead ends and less flooded areas. Therefore, optimized nutrient flow
390 velocity and nutrient concentration could ensure sufficient nutrients supplying rate with moderate shear
391 stress in the pore space, resulting in a fast and stable biofilm accumulation in both flowing and non-flow
392 regions.

Biofilm adhesive strength with the glass surface

The results of qPCR analysis reflect the detachment of biofilm as responding to the stresses from the environment, including shear stress and nutrient starvation [5]. In this study, we observed that the biofilm-dispersal cells increased with flow velocity due to the shear stress induced detachment, and nutrient starvation was also a trigger for biofilm dispersal. In a flowing system, biofilm dispersal is beneficial to spawn novel biofilm development cycles at new locations, which can ensure attachment and bioplug formation developing further into flooded porous media.

In contrast to the planktonic mode, biofilm in a self-generated matrix can behave as viscous liquids to resist the flow shear stress and prevent from detachment from the attached solid surface. The results from biofilm adhesive strength test have demonstrated that biofilm growing at the optimum shear stress could resist the flow-induced shear stress, which is in agree with the results of Park et al.[33] that under the optimum shear stress, EPS structure could provide a mechanical shield to protect biofilm. Compared to the snap-off of initial attachment in the beginning of nutrient injection, the adhesive strength between biofilm and adhesive surface seemed to become stronger under shear [2,31]. However, biofilm growth at high nutrient concentration (20 mM) formed a loose structure with a high accumulation rate but a weak adhesive strength with substrates, which was easily detached by fluid shear.

Conclusion

In summary, this work demonstrates that flow velocity and nutrient concentrations could control biofilm development in porous media in a bioplugging trial. Negligible biofilm formation at the relatively high flow velocity of 4.17 mm/s and low nutrient concentration of 1 mM suggests that there is a ‘no/low growth region’, where the high shear force leads to biofilm detachment and nutrient concentration is below the minimum required for biofilm formation. This is supported by the earlier work [40,41]. At the conditions investigated in this work, a strong plugging effect in the flowing microchannel was obtained at the relatively low flow velocity of 1.66 mm/s and the medium nutrient concentration of 10 mM substrate, which has a fast biofilm accumulation rate and a strong adhesion force to resist increase in the flow-induced shear. This research gives new insights to influences of flow velocity and nutrient concentration on

biofilm development in porous media at porescale, which may aid evaluations of bioplugging in porous systems such as for oil and ground water reservoirs. As potential permeability reducers in oil reservoirs, biofilm accumulation in porous media needs to be controlled by flow velocity and nutrient availability. Optimized nutrient flow velocity and concentration ensures sufficient nutrients supplying rate with moderate shear stress in the pore, resulting in biofilm accumulation in both flowing and non-flow regions. However, too high stress may prevent biofilm formation and removal of adhered biofilm in the porous media. High nutrient concentration is beneficial for biofilm growth, but leads to a weak biofilm adhesive strength, which is easily detached by flow shear from the pores.

Acknowledgements

We wish to thank Edin Alagic, Rikke H. Ulvøen and Tove L. Eide for technical assistance. This work was supported by the Research Council of Norway and industry partner GOE-IP through the project IMMENS no. 255426.

Compliance with ethical standards

Conflict of interest The authors declare no competing financial interests.

References

1. Bester E, Wolfaardt G, Joubert L, Garny K, Saftic S (2005) Planktonic-cell yield of a pseudomonad biofilm. Appl Environ Microbiol 71:7792-7798. doi:10.1128/AEM.71.12.7792-7798.2005

2. Billings N, Birjiniuk A, Samad TS, Doyle PS, Ribbeck K (2015) Material properties of biofilms-a review of methods for understanding permeability and mechanics. Rep Prog Phys 78:036601. doi:10.1088/0034-4885/78/3/036601

3. Brown LR (2010) Microbial enhanced oil recovery (MEOR). Curr Opin Microbiol 13:316-320. doi:10.1016/j.mib.2010.01.011

4. Cherifi T, Jacques M, Quessy S, Fravalo P (2017) Impact of Nutrient Restriction on the Structure of Listeria monocytogenes Biofilm Grown in a Microfluidic System. Front Microbiol 8:864. doi:10.3389/fmicb.2017.00864

443 5. Chua SL, Liu Y, Yam JKH, Chen Y, Vejborg RM, Tan BGC, Kjelleberg S, Tolker-Nielsen T, Givskov
444 M, Yang L (2014) Dispersed cells represent a distinct stage in the transition from bacterial biofilm
445 to planktonic lifestyles. Nature Communications 5. doi:10.1038/ncomms5462
446 6. Cuzman OA, Rescic S, Richter K, Wittig L, Tiano P (2015) Sporosarcina pasteurii use in extreme
447 alkaline conditions for recycling solid industrial wastes. J Biotechnol 214:49-56.
448 doi:10.1016/j.jbiotec.2015.09.011
449 7. David C, Bühler K, Schmid A (2015) Stabilization of single species Synechocystis biofilms by
450 cultivation under segmented flow. J Ind Microbiol Biotechnol 42:1083-1089. doi:10.1007/s10295-
451 015-1626-5
452 8. Dumitrache A, Wolfaardt G, Allen G, Liss SN, Lynd LR (2013) Form and function of Clostridium
453 thermocellum biofilms. Appl Environ Microbiol 79:231-239. doi:10.1128/AEM.02563-12
454 9. Dunsmore BC, Bass CJ, Lappin-Scott HM (2003) A novel approach to investigate biofilm accumulation
455 and bacterial transport in porous matrices. Environmental Microbiology 6:183-187.
456 doi:10.1046/j.1462-2920.2003.00546.x
457 10. Ezeuko CC, Sen A, Gates ID (2013) Modelling biofilm-induced formation damage and biocide
458 treatment in subsurface geosystems. Microbial biotechnology 6:53-66. doi:10.1111/1751-
459 7915.12002
460 11. Flemming H-C, Wingender J, Szewzyk U (2011) Biofilm highlights, vol 5. Springer Series on Biofilms.
461 Heidelberg, USA
462 12. Franco-Rivera A, Paniagua-Michel J, Zamora-Castro J (2007) Characterization and performance of
463 constructed nitrifying biofilms during nitrogen bioremediation of a wastewater effluent. J Ind
464 Microbiol Biotechnol 34:279-287. doi:10.1007/s10295-006-0196-y
465 13. Fujiwara K, Sugai Y, Yazawa N, Ohno K, Hong CX, Enomoto H (2004) Biotechnological approach for
466 development of microbial enhanced oil recovery technique. Petroleum Biotechnology:
467 Developments and Perspectives 151:405-445
468 14. Garrett TR, Bhakoo M, Zhang Z (2008) Bacterial adhesion and biofilms on surfaces. Progress in
469 Natural Science 18:1049-1056. doi:https://doi.org/10.1016/j.pnsc.2008.04.001

15. Hao R, Meng C, Li J (2017) Impact of operating condition on the denitrifying bacterial community structure in a 3DBER-SAD reactor. J Ind Microbiol Biotechnol 44:9-21. doi:10.1007/s10295-016-1853-4

16. Hosseininoosheri P, Lashgari HR, Sepehrnoori K (2016) A novel method to model and characterize in-situ bio-surfactant production in microbial enhanced oil recovery. Fuel 183:501-511. doi:10.1016/j.fuel.2016.06.035

17. Hsi CD, Dudzik DS, Lane RH, Buettner JW, Neira RD (1994) Formation Injectivity Damage Due to Produced Water Reinjection. Paper presented at the SPE Formation Damage Control Symposium, Lafayette, Louisiana, 1994/1/1/

18. Hunt SM, Werner EM, Huang B, Hamilton MA, Stewart PS (2004) Hypothesis for the role of nutrient starvation in biofilm detachment. Appl Environ Microbiol 70:7418-7425. doi:10.1128/AEM.70.12.7418-7425.2004

19. Joshi S, Goyal S, Mukherjee A, Reddy MS (2017) Microbial healing of cracks in concrete: a review. J Ind Microbiol Biotechnol 44:1511-1525. doi:10.1007/s10295-017-1978-0

20. Karambeigi MS, Schaffie M, Fazaelipoor MH (2013) Improvement of Water Flooding Efficiency Using Mixed Culture of Microorganisms in Heterogeneous Micro-models. Petroleum Science and Technology 31:923-931. doi:10.1080/10916466.2010.506461

21. Karimi M, Mahmoodi M, Niazi A, Al-Wahaibi Y, Ayatollahi S (2012) Investigating wettability alteration during MEOR process, a micro/macro scale analysis. Colloids Surf B Biointerfaces 95:129-136. doi:10.1016/j.colsurfb.2012.02.035

22. Khajepour H, Mahmoodi M, Biria D, Ayatollahi S (2014) Investigation of wettability alteration through relative permeability measurement during MEOR process: A micromodel study. J Pet Sci Eng 120:10-17. doi:10.1016/j.petrol.2014.05.022

23. Kirby BJ (2010) Passive Scalar Transport: Dispersion, Patterning, and Mixing. In: Micro- and Nanoscale Fluid Mechanics: Transport in Microfluidic Devices. Cambridge University Press, New York. doi:https://doi.org/10.1017/CBO9780511760723.006

496 24. Klueglein N, Kögler F, Adaktylou IJ, Wuestner ML, Mahler E, Scholz J, Herold A, Alkan H (2016)
497 Understanding Selective Plugging and Biofilm Formation of a Halophilic Bacterial Community
498 for MEOR Application. Society of Petroleum Engineers SPE-179620-MS
499 25. Lam RH, Cui X, Guo W, Thorsen T (2016) High-throughput dental biofilm growth analysis for
500 multiparametric microenvironmental biochemical conditions using microfluidics. Lab Chip
501 16:1652-1662. doi:10.1039/c6lc00072j
502 26. Landa-Marbán D, Liu N, Pop IS, Kumar K, Pettersson P, Bødtker G, Skauge T, Radu FA (2018) A
503 Pore-Scale Model for Permeable Biofilm: Numerical Simulations and Laboratory Experiments.
504 Transport in Porous Media. doi:10.1007/s11242-018-1218-8
505 27. Lane DJ (1991) 16S/23S rRNA sequencing. In: Stackebrandt E, Goodfellow M (eds) Nucleic acid
506 techniques in bacterial systematics. Wiley, London, pp 115-175
507 28. Lee JH, Kaplan JB, Lee WY (2008) Microfluidic devices for studying growth and detachment of
508 Staphylococcus epidermidis biofilms. Biomed Microdevices 10:489-498. doi:10.1007/s10544-
509 007-9157-0
510 29. Muyzer G, Dewaal EC, Uitterlinden AG (1993) Profiling of complex microbial-populations by
511 denaturing gradient gel-electrophoresis analysis of polymerase chain reaction-amplified genes-
512 coding for 16S ribosomal-RNA. Appl Environ Microb 59:695-700
513 30. Myhr S, Lillebo BL, Sunde E, Beeder J, Torsvik T (2002) Inhibition of microbial H2S production in an
514 oil reservoir model column by nitrate injection. Appl Microbiol Biotechnol 58:400-408.
515 doi:10.1007/s00253-001-0881-8
516 31. Ohashi A, Harada H (1994) Adhesion strength of biofilm developed in an attached-growth reactor.
517 Water Science and Technology 29:8
518 32. Oka GK, Pinder GF (2017) Multiscale Model for Assessing Effect of Bacterial Growth on Intrinsic
519 Permeability of Soil: Model Description. Transport Porous Med 119:267-284.
520 doi:10.1007/s11242-017-0870-8
521 33. Park A, Jeong H-H, Lee J, Kim KP, Lee C-S (2011) Effect of shear stress on the formation of bacterial
522 biofilm in a microfluidic channel. BioChip Journal 5:236-241. doi:10.1007/s13206-011-5307-9

34. Peszynska M, Trykozko A, Iltis G, Schlueter S, Wildenschild D (2016) Biofilm growth in porous media: Experiments, computational modeling at the porescale, and upscaling. Adv Water Resour 95:288-301. doi:10.1016/j.advwatres.2015.07.008

35. Rabiei A, Sharifinik M, Niazi A, Hashemi A, Ayatollahi S (2013) Core flooding tests to investigate the effects of IFT reduction and wettability alteration on oil recovery during MEOR process in an Iranian oil reservoir. Appl Microbiol Biotechnol 97:5979-5991. doi:10.1007/s00253-013-4863-4

36. Rochex A, Lebeault JM (2007) Effects of nutrients on biofilm formation and detachment of a Pseudomonas putida strain isolated from a paper machine. Water Res 41:2885-2892. doi:10.1016/j.watres.2007.03.041

37. Rukavina Z, Vanic Z (2016) Current Trends in Development of Liposomes for Targeting Bacterial Biofilms. Pharmaceutics 8. doi:10.3390/pharmaceutics8020018

38. Sarafzadeh P, Niazi A, Oboodi V, Ravanbakhsh M, Hezave AZ, Ayatollahi SS, Raeissi S (2014) Investigating the efficiency of MEOR processes using Enterobacter cloacae and Bacillus stearothermophilus SUCPM#14 (biosurfactant-producing strains) in carbonated reservoirs. J Pet Sci Eng 113:46-53. doi:10.1016/j.petrol.2013.11.029

39. Skolimowski M, Nielsen MW, Emneus J, Molin S, Taboryski R, Sternberg C, Dufva M, Geschke O (2010) Microfluidic dissolved oxygen gradient generator biochip as a useful tool in bacterial biofilm studies. Lab Chip 10:2162-2169. doi:10.1039/c003558k

40. Stoodley P, Cargo R, Rupp CJ, Wilson S, Klapper I (2002) Biofilm material properties as related to shear-induced deformation and detachment phenomena. J Ind Microbiol Biotechnol 29:361-367. doi:10.1038/sj.jim.7000282

41. Stoodley P, Dodds I, J.D. B, H.M. L-S (1999) Influence of hydrodynamics and nutrients on biofilm structure. J Appl Microbiol 85:7

42. Sun D-L, Jiang X, Wu QL, Zhou N-Y (2013) Intragenomic Heterogeneity of 16S rRNA Genes Causes Overestimation of Prokaryotic Diversity. Applied and Environmental Microbiology 79:5962-5969. doi:doi:10.1128/AEM.01282-13

43. Sunde E, Thorstenson T, Torsvik T (1990) Growth of bacteria on water injection additives. Soc Petrol Eng SPE 20690:301-316

44. Suthar H, Krushi Hingurao, Anjana Desai, Nerurkar aA (2009) Selective Plugging Strategy Based Microbial Enhanced Oil Recovery Using Bacillus licheniformis TT33. J Microbiol Biotechnol 19:8. doi:10.4014/jmb.0904.04043

45. Tahirbegi IB, Ehgartner J, Sulzer P, Zieger S, Kasjanow A, Paradiso M, Strobl M, Bouwes D, Mayr T (2017) Fast pesticide detection inside microfluidic device with integrated optical pH, oxygen sensors and algal fluorescence. Biosens Bioelectron 88:188-195. doi:10.1016/j.bios.2016.08.014

46. Tsai YP (2005) Impact of flow velocity on the dynamic behaviour of biofilm bacteria. Biofouling 21:267-277. doi:10.1080/08927010500398633

47. Vilcáez J, Li L, Wu D, Hubbard SS (2013) Reactive Transport Modeling of Induced Selective Plugging byLeuconostoc Mesenteroidesin Carbonate Formations. Geomicrobiol J 30:813-828. doi:10.1080/01490451.2013.774074

48. Weiss N, Obied KE, Kalkman J, Lammertink RG, van Leeuwen TG (2016) Measurement of biofilm growth and local hydrodynamics using optical coherence tomography. Biomed Opt Express 7:3508-3518. doi:10.1364/BOE.7.003508

49. Yawata Y, Nguyen J, Stocker R, Rusconi R (2016) Microfluidic Studies of Biofilm Formation in Dynamic Environments. J Bacteriol 198:2589-2595. doi:10.1128/JB.00118-16

50. Yuan B, Wood DA (2018) Chapter One - Overview of Formation Damage During Improved and Enhanced Oil Recovery. In: Yuan B, Wood DA (eds) Formation Damage During Improved Oil Recovery. Gulf Professional Publishing, pp 1-20. doi:https://doi.org/10.1016/B978-0-12-813782-6.00001-4

51. Zhang YD, Li C, Wu YC, Zhang YL, Zhou Z, Cao B (2019) A microfluidic gradient mixer-flow chamber as a new tool to study biofilm development under defined solute gradients. Biotechnology and Bioengineering 116:54-64. doi:10.1002/bit.26852